

The HARPS search for southern extra-solar planets[★]

XX. Planets around the active star BD −08°2823

G. Hébrard¹, S. Udry², G. Lo Curto³, N. Robichon⁴, D. Naef^{2,5}, D. Ehrenreich^{1,6}, W. Benz⁷, F. Bouchy^{1,8},
A. Lecavelier des Etangs¹, C. Lovis², M. Mayor², C. Moutou⁹, F. Pepe², D. Queloz², N. C. Santos¹⁰, D. Ségransan³

¹ Institut d’Astrophysique de Paris, UMR7095 CNRS, Université Pierre & Marie Curie, 98bis boulevard Arago, 75014 Paris, France

² Observatoire de Genève, Université de Genève, 51 Chemin des Maillettes, 1290 Sauverny, Switzerland

³ ESO, Karl-Schwarzschild-Strasse 2, D-85748 Garching bei München, Germany

⁴ Observatoire de Paris, GEPI, 5 Place Jules Janssen, F-92195 Meudon, France

⁵ ESO, Alonso de Cordoba 3107, Vitacura Casilla 19001, Santiago, Chile

⁶ Laboratoire d’Astrophysique de Grenoble, CNRS (UMR 5571), Université J. Fourier, BP53, 38041 Grenoble cedex 9, France

⁷ Physikalisches Institut Universität Bern, Sidlerstrasse 5, 3012 Bern, Switzerland

⁸ Observatoire de Haute-Provence, CNRS/OAMP, 04870 Saint-Michel-l’Observatoire, France

⁹ Laboratoire d’Astrophysique de Marseille, Université de Provence, CNRS (UMR 6110), BP 8, 13376 Marseille Cedex 12, France

¹⁰ Centro de Astrofísica, Universidade do Porto, Rua das Estrelas, 4150-762 Porto, Portugal

Received TBC; accepted TBC

ABSTRACT

We report the detection of a planetary system around BD −08°2823, that includes at least one Uranus-mass planet and one Saturn-mass planet. This discovery serendipitously originates from a search for planetary transits in the *Hipparcos* photometry database. This program preferentially selected active stars and did not allow the detection of new transiting planets. It allowed however the identification of the K3V star BD −08°2823 as a target harboring a multiplanet system, that we secured and characterized thanks to an intensive monitoring with the HARPS spectrograph at the 3.6-m ESO telescope in La Silla. The stellar activity level of BD −08°2823 complicates the analysis but does not prohibit the detection of two planets around this star. BD −08°2823b has a minimum mass of $14.4 \pm 2.1 M_{\oplus}$ and an orbital period of 5.60 days, whereas BD −08°2823c has a minimum mass of $0.33 \pm 0.03 M_{\text{Jup}}$ and an orbital period of 237.6 days. This new system strengthens the fact that low-mass planets are preferentially found in multiplanetary systems, but not around high-metallicity stars as this is the case for massive planets. It also supports the belief that active stars should not be neglected in exoplanet searches, even when searching for low-mass planets.

Key words. planetary systems – techniques: radial velocities – stars: individual: BD −08°2823

1. Introduction

The HARPS spectrograph (Mayor et al. 2003) is operating since 2003 at the 3.6-m ESO telescope in La Silla, Chile. This is a fiber-fed, environmentally stabilized high-resolution echelle spectrograph dedicated to high-precision radial velocity measurements. Thanks to the exoplanetology programs that are conducted with it, it allowed numerous extra-solar planets studies and discoveries, in the ranges of Jupiter-mass planets (e.g. Pepe et al. 2004, Moutou et al. 2009a), low-mass planets (e.g. Lovis et al. 2006, Mayor et al. 2009), planets around early- (e.g. Desort et al. 2008, Lagrange et al. 2009) or late-type stars (e.g. Bonfils et al. 2007, Forveille et al. 2009), or transiting planets (e.g. Bouchy et al. 2008, Queloz et al. 2009). The essential quality of HARPS (the High Accuracy Radial velocity Planet Searcher) is its high stability, which results in a $\text{sub-}m\text{s}^{-1}$ accuracy in the radial velocity measurements, on time-scales of several years. This allows the detection of planets in the Neptune or Super-Earth mass ranges, on progressively increasing orbital periods as the time-span of the monitoring is growing up. This instrument

hitherto plays a major role in the improvement of the knowledges of exoplanets.

We report here the detection of a new multiplanetary system. It serendipitously originates from the radial velocity follow-up accompanying a search for planetary transits in the *Hipparcos* epoch photometry annex (Perryman et al. 1997). Despite its significant stellar activity, the star BD −08°2823 was identified during this follow-up as a possible host of extra-solar planets. An intensive monitoring of its radial velocities was subsequently carried out with HARPS, that led to the detection of a planetary system around this star, including at least two planets. We briefly present the search for planetary transits in the *Hipparcos* photometry in § 2. The HARPS observations of BD −08°2823 are presented in § 3 together with the stellar properties of this target. The planetary system is characterized in § 4, then the results are discussed in § 5.

2. Search for transiting planets in the *Hipparcos* database

The goal of our initial search in the *Hipparcos* database was to try to find new transiting planets, especially around bright stars. Transiting planets could allow numerous important studies to be performed. These studies include planetary radii, masses and

[★] Based on observations made with HARPS spectrograph on the 3.6-m ESO telescope at La Silla Observatory, Chile, under the programs ID 072.C-0488, 074.C-0364 and 078.C-0044.

densities measurements, accurate determination of the inclinations and the eccentricities of the orbits, possible detections of transit timing variations due to additional companions, measurements of the spin-orbit (mis)alignment angles, detections of the emission or absorption planetary spectra, or even satellites or rings detections. The famous planets transiting in front of the bright stars HD 209458 and HD 189733 are those that allow the most accurate measurements and the deepest investigations.

The *Hipparcos* epoch photometry annex contains between ~ 40 and ~ 300 photometric measurements performed during the 1226-day duration of the mission for each of the 118 204 stars of the catalog, in the magnitude limit $V \leq 10$. With about 0.1% chance that a given star harbors a transiting extra-solar planet, the *Hipparcos* all-sky survey must contain photometric measurements for tens of transiting hot Jupiters. This belief is reinforced by the two cases of transiting planets *a posteriori* re-discovered in *Hipparcos* data: HD 209458b (Robichon & Arenou 2000, Castellano et al. 2000, Söderhjelm 1999) and HD 189733b (Bouchy et al. 2005, Hébrard & Lecavelier des Etangs 2006). Thanks to the long time baseline, these data also allow the orbital period to be measured with an accuracy of the order of the second.

Up to now, there are the only two transiting planets that have been found in the *Hipparcos* database. Indeed, with photometric variations of about 1% or less, such transits are difficult to identify in the *Hipparcos* data, that present a mean photometric accuracy of the same order of magnitude. The poor time coverage, by comparison with dedicated surveys as SuperWASP, XO, CoRoT or Kepler, is another difficulty. Jenkins et al. (2002) concluded that because of its poor photometric quality, the *Hipparcos* catalog does not represent a likely place to detect planets in the absence of other informations. It might however provide planetary transit candidates for follow-up observations. Laughlin (2000) has searched in the *Hipparcos* epoch photometry for transiting planets within 206 metal-rich stars. None have been confirmed thereafter.

We present in Appendix A the systematic search we managed in the *Hipparcos* epoch photometry annex for periods compatible with planetary transits. We constructed a ranked list of candidates for follow-up radial velocity measurements, based on the depth and significance of the planetary transits that could be detected in the *Hipparcos* photometry. The simulations we performed indicated that our detection rate for transiting planets is low, of the order of 2%; so the chances to find new transiting planets in the *Hipparcos* data are small (see Appendix A). However, the particularly high interest for the potential discovery of a planet transiting a bright star pushed us to perform a radial velocity follow-up of our candidates.

We observed 194 of these selected, ranked targets with HARPS, in order to search for radial velocity variations in agreement with the transiting candidates found in the *Hipparcos* photometry. The HARPS setup, the spectra extraction and the radial velocity measurements were identical to those described below in § 3.1. Most of these observations were performed in December 2004 as part of the program 074.C-0364. Radial velocity variations larger than 20 m s^{-1} were measured for 37 stars, i.e. 19% of our observed sample. Those variations are mainly caused by stellar activity. Indeed, most of the targets with large radial velocity variations show emissions in the Ca II H & K lines (3934.8 \AA and 3969.6 \AA). The level of these emissions is quantified with the activity S-index (Mount Wilson System), which is converted to the $\log R'_{\text{HK}}$ index (Santos et al. 2000). The majority of the variable targets have $\log R'_{\text{HK}}$ indexes larger than -4.7 , in-

dicating prominent chromospheric activity; this can explain such level of radial velocity variations (Santos et al. 2000).

Some targets first seemed to exhibit periodic radial velocity variations, but subsequent monitoring with HARPS showed that these variations were not persistent with time, in agreement with transient activity processes on the stellar surface due to activity (flares, spots, plages...) modulated by the stellar rotation. In addition, in most of the cases, analysis of the line profiles using bisectors of the cross-correlation functions shown variations in the shape of the lines with time. This indicates that the observed radial velocity variations are not due to Doppler shifts of the lines, but rather to deformations of the shape of the spectral lines. Some cases revealed a clear anti-correlation between radial velocity and line-bisector orientation, which could be understood as the signature of cool spots on the stellar photospheres (see, e.g., Queloz et al. 2001, Melo et al. 2007, Desort et al. 2007, Boisse et al. 2009).

Thus, our procedure seems to preferentially select active stars. This should be contrasted with transiting candidates obtained from the photometric surveys dedicated to transiting planet searches, which are mainly eclipsing binaries or transiting planets (see, e.g., Pont et al. 2005). None of the targets that we observed through this program have shown radial velocity variations in agreement with a reflex motion due to a hot Jupiter. Instead, most of the radial velocity variations seem to be caused by stellar activity.

However, these observations allowed the serendipitously discovery of a new planetary system, without transit detection in the *Hipparcos* data. This system orbits BD−08°2823, which is an active star, but among those with the lowest $\log R'_{\text{HK}}$ indexes within our monitored targets. This activity level complicates planet detection but does not prohibit it in this case. We concentrate below on this target and the detection of its harbored planetary system.

3. Observations and properties of BD−08°2823

3.1. HARPS observations of BD−08°2823

We observed BD−08°2823 using the HARPS spectrograph at the 3.6-m ESO telescope in La Silla. The bandpass of the spectra ranges from 3800 \AA to 6900 \AA , and the resolution power is $R = 115\,000$, with a fiber diameter of 1 arcsec. The spectra were extracted from the detector images with the HARPS pipeline, that includes localization of the orders on the 2D-images, optimal order extraction, cosmic-ray rejection, wavelength calibration and corrections of flat-field. The pipeline then performs a cross-correlation of the extracted spectra with a numerical mask (K5-type in this case), and finally measures the radial velocities from Gaussian fits of the cross-correlation functions (CCFs), following the method described by Baranne et al. (1996) and Pepe et al. (2002). The full dataset we use for BD−08°2823 includes 83 spectra. All the exposures (but the first one) were obtained without simultaneous thorium calibration. The exposure times for BD−08°2823 range between 4 and 15 minutes, allowing a signal-to-noise ratio per pixel between 30 and 80 to be reached around 550 nm . The total exposure time is about 11 hours.

The HARPS radial velocities of BD−08°2823 as a function of time are plotted in the upper panel of Fig. 1. They span 1841 days, corresponding to 5.0 years. A few measurements were obtained in late-2004 as part of the program 074.C-0364 (see § 2), then the target was regularly monitored. A few extra measurements were acquired in late-2006/early-2007 as part of the program 078.C-0044, but most of the data were secured as

part of the *Guaranteed Time Observations* (GTO) survey program 072.C-0488 (Mayor et al. 2003). This is the case in particular for the intensive series in 2007–2008 (BDJ−2 400 000 between 54 150 and 54 650). There was indeed an agreement to follow, as part of the GTO time, a few promising targets identified from the *Hipparcos* original program.

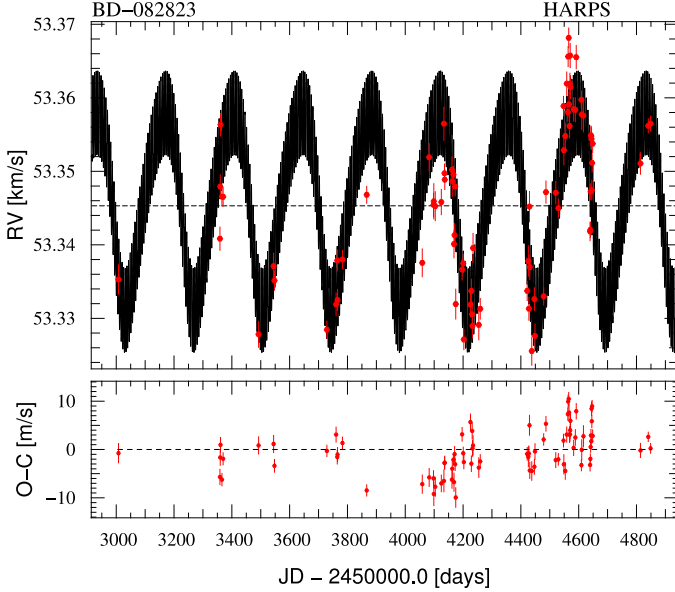


Fig. 1. *Top:* Radial velocity HARPS measurements of BD−08°2823 as a function of time (see § 3), and Keplerian fit with two planets (see § 4). The orbital parameters corresponding to this fit are reported in Table 3. *Bottom:* Residuals of the fit with 1- σ error bars.

The derived radial velocities are reported in Table 1. The accuracies are between 1.0 and 2.4 m s^{−1}, typically around 1.6 m s^{−1}. This includes photon noise but not the jitter due to stellar oscillations or activity (§ 3.2). Wavelength calibration and spectrograph drift uncertainties are negligible with respect to the photon noise. Four exposures with radial velocity uncertainties larger than 2.4 m s^{−1} were not included in the final dataset of 83 spectra.

The radial velocities show a significant 11-m s^{−1} dispersion (43 m s^{−1} peak-to-peak), well over the expected accuracy (Fig. 1, upper panel). The CCF from which those radial velocities were measured show parameters that also significantly vary with time. Their full widths at half maximum fluctuates between 6.22 ± 0.01 and 6.33 ± 0.01 km s^{−1}, and their contrasts from 46.80 ± 0.05 and 47.50 ± 0.05 % of the continuum. The bisector span of the CCF also show a dispersion, at the level of 7 m s^{−1} (see Fig. 2, upper panel). Thus, Doppler shifts of the spectral lines of BD−08°2823 are not necessarily the only explanation for the observed radial velocity variations; changes in the shape of the lines, as those due to stellar activity, are likely to be the cause of at least a part of those variations.

3.2. Stellar properties and activity

Table 2 summarizes the stellar parameters of BD−08°2823 (HIP 49067, SAO 137286). According to the SIMBAD database, this is K3V star of magnitude $V = 9.86$. Its *Hipparcos* parallax

Table 1. HARPS measurements of BD−08°2823 (full table available electronically)[†].

BJD −2 400 000	RV km s ^{−1}	σ (RV) km s ^{−1}	FWHM km s ^{−1}	Bis. km s ^{−1}	$\log R'_{\text{HK}}$
53007.83343	53.3353	0.0020	6.281	0.0222	−4.702
53358.83576	53.3408	0.0016	6.248	0.0183	−4.731
53359.80161	53.3479	0.0016	6.255	0.0154	−4.725
53360.81961	53.3563	0.0015	6.252	0.0226	−4.742
...
...
54648.45269	53.3538	0.0012	6.322	0.0326	−4.709
54813.83365	53.3511	0.0015	6.291	0.0273	−4.755
54840.78987	53.3562	0.0010	6.300	0.0294	−4.732
54848.79967	53.3565	0.0010	6.283	0.0257	−4.751

[†]: the six columns are respectively the Barycentric Julian Day of the observations, the radial velocity and its uncertainty, the full width at half maximum of the CCF, the span of its bisector, and the Ca II activity index.

($\pi = 23.76 \pm 1.61$ mas) implies a distance of 42.2 ± 2.9 pc. The *Hipparcos* color is $B - V = 1.071 \pm 0.010$. From spectral analysis of the HARPS data using the method presented in Santos et al. (2004a), we derive the temperature $T_{\text{eff}} = 4746 \pm 63$ K, the gravity $\log g = 4.13 \pm 0.26$, the metallicity $[\text{Fe}/\text{H}] = -0.07 \pm 0.03$, and an uncertain age of 4.5 ± 4.0 Gyr. The stellar mass we obtain is $M_* = 0.74 M_{\odot}$, with a formal error bar of $\pm 0.2 M_{\odot}$. Following Fernandes & Santos (2004), we rather adopt a conservative ± 10 % uncertainty, corresponding to $\pm 0.07 M_{\odot}$. We derive a projected rotational velocity $v \sin i_* = 1.4$ km s^{−1} from the parameters of the CCF using a calibration similar to that presented by Santos et al. (2002). Acoustic oscillations are not averaged out in the data, as there are on timescales similar or shorter than the exposure times we used. However, for a K-type star, oscillation amplitudes are expected to be negligible by comparison with stellar activity effects on the measured radial velocities.

Table 2. Stellar parameters for BD−08°2823.

Parameters	Values
m_v	9.86
Spectral type	K3V
$B - V$	1.071 ± 0.010
Parallax [mas]	23.76 ± 1.61
Distance [pc]	42.2 ± 2.9
$v \sin i_*$ [km s ^{−1}]	1.4
P_{rot} [days]	26.6 ± 1.5
$\log R'_{\text{HK}}$	-4.8 ± 0.1
[Fe/H]	-0.07 ± 0.03
T_{eff} [K]	4746 ± 63
$\log g$ [cgs]	4.13 ± 0.26
Mass [M_{\odot}]	0.74 ± 0.07
Age [Gyr]	4.5 ± 4.0

The core of the large H & K Ca II absorption lines of BD−08°2823 show emissions, indicating chromospheric activity. We adopted the averaged value $\log R'_{\text{HK}} = -4.8 \pm 0.1$, but it significantly varies with time, between extrema $\log R'_{\text{HK}} = -4.68 \pm 0.01$ and -4.88 ± 0.01 . Such stellar activity would imply a significant jitter on the observed stellar radial velocities. For a K-type star with this level of activity, Santos et al. (2000) predict a dispersion up to 10 m s^{−1} for the stellar jitter. This is the order of magnitude of the dispersion of our measurements of BD−08°2823 (§ 3.1). A classic method to identify stellar ac-

tivity as the main cause of radial velocity variations is to look for anti-correlation between radial velocity and the bisector span (see, e.g., Queloz et al. 2001, Boisse et al. 2009). The upper panel of Fig. 2 shows the bisector spans as a function of the radial velocities for BD−08°2823. As seen above, the bisector is significantly varying; however, no clear relations are seen between the two signals. Yet, this technic is less sensitive for stars with slow rotations, as this is the case for BD−08°2823. Indeed, according to Noyes et al. (1984) and Mamajek & Hillenbrand (2008), the activity level for BD−08°2823 implies a stellar rotation period around 37 days. The *Hipparcos* data of BD−08°2823 includes photometric measurements for 63 epochs only; this does not allow a rotation period measurement.

A different estimation of the rotation period could be obtained from the HARPS data through the stellar activity indicators, as shown in Fig. 3. In this figure are plotted the Lomb-Scargle periodograms (Press et al. 1992) of five HARPS signals: the radial velocities, full widths at half maximum (FWHMs), contrasts and bisectors of the CCFs, and of the $\log R'_{\text{HK}}$ activity indexes (Table 1). The fourth last parameters could show signatures of the stellar activity, and in particular their modulations with the stellar rotation; the radial velocity variations could as well show signatures of the stellar activity and rotation, but also the Doppler reflex motion due to companion(s). The five periodograms in Fig. 3 all clearly show a peak around 26 days. We interpret it as the signature of modulations of the stellar surface due to activity (flares, spots, plages...). This kind of phenomena are expected for such an active star. As there are sporadic events altering the surface of the star and having limited life times, they would imply quasi-periodic variations of the shapes of the spectral lines, with periods near the stellar rotation period, and un-conserved phases. The rotation period of BD−08°2823 seems thus to be around 26 days from these data. Most of the signals show also a small peak near 13-days, which is the first harmonic of the main signal; it is not detected in the radial velocities, however. In addition, the five periodograms in Fig. 3 show signal between 65 and 95 days. It may be the signature of the typical duration of cycles of these phenomena.

The radial velocity periodogram show two extra peaks that are not seen for other signals in Fig. 3, at 5.6 and 238 days. The fact that these periodic signals are detected only in radial velocities suggests it is caused by Doppler reflex motion due to companions for BD−08°2823 rather than jitter due to stellar activity. Moreover, those two periods do not correspond to any harmonics nor aliases of the 26 days rotation period. The amplitude of the variations (43 m s^{-1} peak-to-peak, see upper panel of Fig. 1) and the two orbital periods (near 5.6 and 238 days) imply projected masses $M_{\text{p}} \sin i$ well below the mass of Jupiter. The radial velocity variations detected by HARPS would thus originate both from stellar activity jitter and planetary companions.

4. A planetary system around BD−08°2823

4.1. Fit without stellar activity

We first fitted the radial velocities using a two-planet Keplerian model without mutual interactions. The results are plotted in Figs. 1 and 4. The inner planet, BD−08°2823b, produces radial velocity variations with a small semi-amplitude $K = 6.5 \text{ m s}^{-1}$, corresponding to a planet with a minimum mass $M_{\text{p}} \sin i = 14.4 M_{\oplus}$, thus similar to the mass of Uranus. Its orbit has a period of 5.60 days and is circular or with low eccentricity. The outer planet, BD−08°2823c, yields a larger semi-amplitude, namely $K = 13.4 \text{ m s}^{-1}$; this corresponds to a planet with a minimum

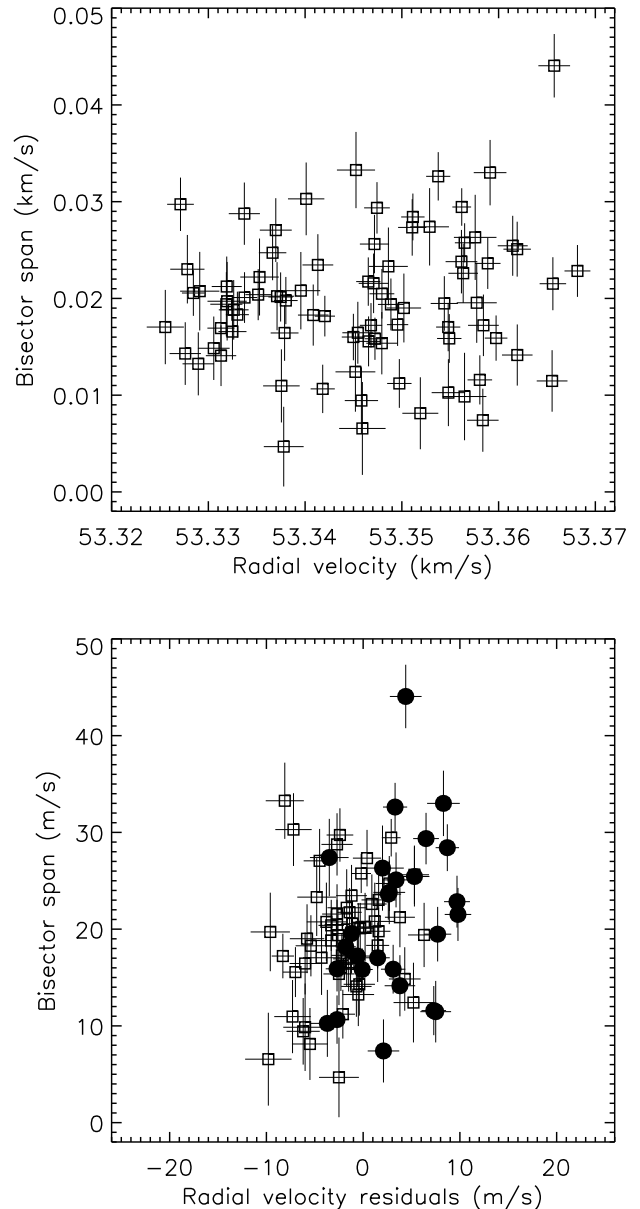


Fig. 2. Bisector span as a function of the radial velocity (upper panel) and of the residuals of the fit with two planets as shown in Figs. 1 and 4 (lower panel). On the lower panel, the filled circles indicate the measurements secured on the 101-day interval, where we fitted the stellar jitter (§ 4.2 and Fig. 6). The ranges have the same extends in x - and y -axes on both panels.

mass $M_{\text{p}} \sin i = 0.33 M_{\text{Jup}}$, slightly above the Saturn mass. The orbital period is 237.6 days, and the orbit is non-circular ($e = 0.19$). The derived orbital parameters of the system are summarized in Table 3.

The reduced χ^2 of the Keplerian fit is 3.2, and the standard deviation of the residuals is $\sigma_{\text{O-C}} = 4.3 \text{ m s}^{-1}$. This is reduced when compared to the 11-m s^{-1} dispersion of the original radial velocities, but this is clearly higher than the 1.6-m s^{-1} typical error bars on the individual measurements. The extra dispersion, of the order of 4 m s^{-1} , is mainly due to stellar activity jitter as seen above. By fitting the two planets without including the stellar ac-

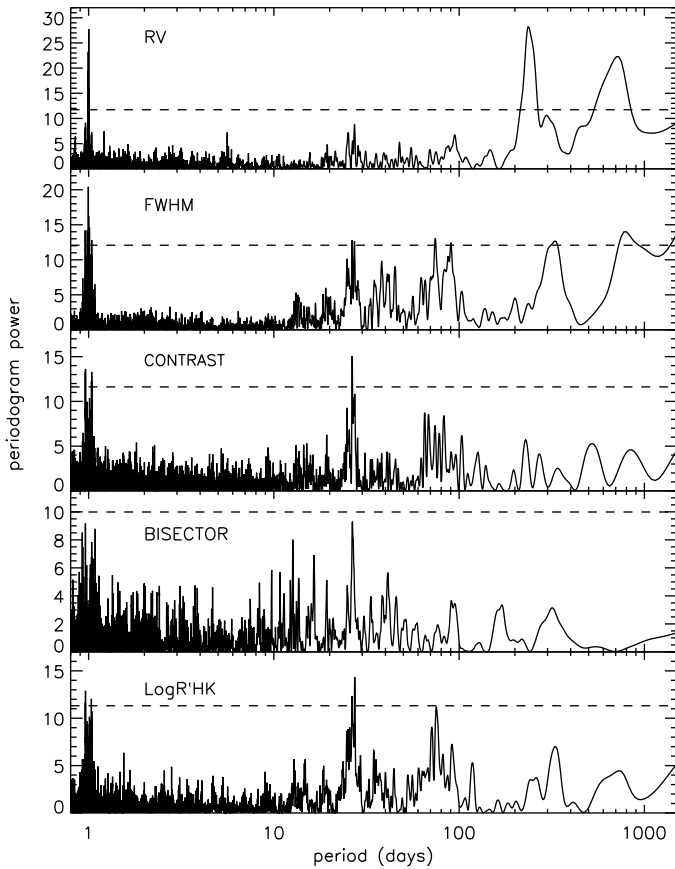


Fig. 3. Lomb-Scargle periodograms for BD−08°2823 HARPS signals. From top to bottom, the five panels show the periodograms of the radial velocities, of the FWHMs, contrasts and bisectors of the CCFs, and finally of the $\log R'_{\text{HK}}$ activity indexes. Each of these five signals shows a peak in the power around 26 days, which could be interpreted as the stellar rotation period. On the upper panel, the radial velocities periodogram shows two extra peaks at 5.6 and 238 days, which are not seen in the four other panels. The horizontal dashed lines correspond to the false-alarm probability of 1×10^{-3} .

tivity, we assume that the stellar jitter would be averaged out over the five years of observations, as activity induces quasi-periodic effects that are not exactly duplicated in time with the stellar rotation. This results in a quite large dispersion around the fit with respect to the error bars, whereas the periodic signal of the two planets remains coherent over the five years of observations.

Fig. 5 strengthens the interpretation in term of planets of the two signals at 5.6 and 238 days. The upper panel shows the periodogram of the radial velocities, exactly as the upper panel of Fig. 3. On the second panel of Fig. 5 is shown the periodogram of the radial velocity residuals, after a fit including BD−08°2823c only. The standard deviation of the residuals of this fit is $\sigma_{\text{O-C}} = 5.9 \text{ m s}^{-1}$. On this periodogram, the peak at 238 days of course is no longer visible. The main peak is this at 5.6 days. Its false-alarm probability is 5.8×10^{-5} . It is clearly stronger than the peaks due to activity. We note also the presence of two other peaks, at 0.8 and 1.2 day, that are the one-day aliases of the 5.6-day signal in the frequency space ($1 \pm 1/5.6$).

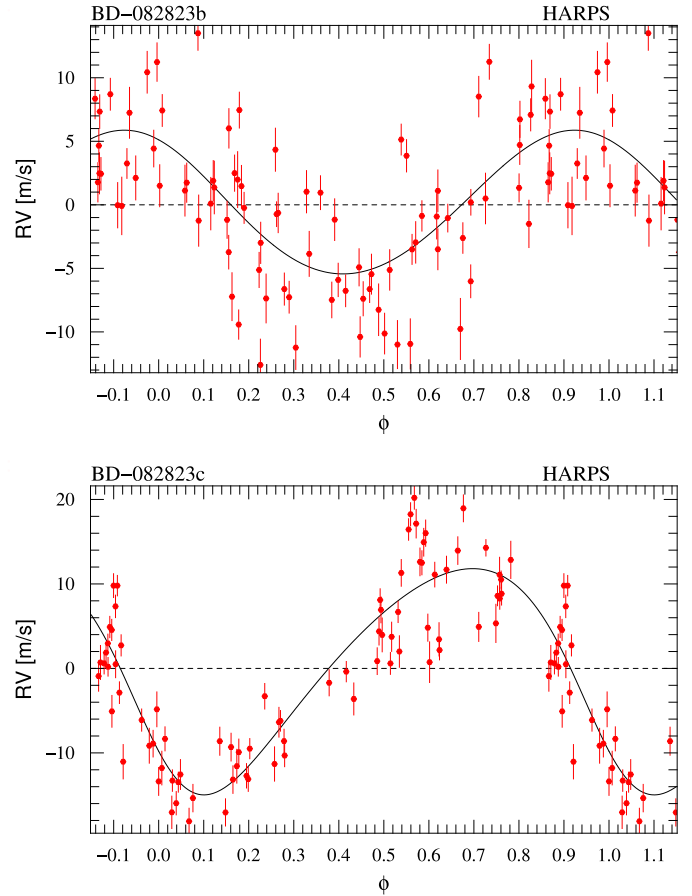


Fig. 4. Phase-folded radial velocity curves for BD−08°2823b ($P = 5.60 \text{ d}$, top) and BD−08°2823c ($P = 237.6 \text{ d}$, bottom) after removing the effect of the other planet. The HARPS radial velocity measurements are presented with $1\text{-}\sigma$ error bars, and the Keplerian fits are the solid lines. Orbital parameters corresponding to the fits are reported in Table 3.

We adopted 5.6 days as the actual period of this signal instead of one of the two aliases, because it is more likely according to the sampling. In addition, its peak is higher than those of the two aliases, and Keplerian fits performed with 0.8 or 1.2 day of orbital periods produce higher residuals dispersion, and eccentric orbits.

Similarly, the third panel of Fig. 5 shows the periodogram of the radial velocity residuals, after a fit including BD−08°2823b only. The peak at 5.6 days is removed as well as its aliases, and the 238-day signal remains, clearly above the activity peaks. Finally, the bottom panel of Fig. 5 shows the periodogram of the residuals after the 2-planet fit shown in Figs. 1 and 4. Only lower peaks are remaining, most of them being caused by activity. Their false-alarm probabilities are larger than of 1×10^{-3} . We note that in addition to the clear peak at one day (which is due to the aliases of all the detected signals), all the four panels in Fig. 5 show a possible peak near 700 days; this could be the signature of a third, outer planet. Fits with a curvature in addition to the two planets also suggest a possible long-period signal (without significant effects on the parameters of BD−08°2823b and BD−08°2823c). Such long-period signals are not strong enough however to claim any detection. Further observations of this tar-

Table 3. Fitted orbits and planetary parameters for the BD−08°2823 system, with 1- σ error bars.

Parameters	BD−08°2823b	BD−08°2823c
P [days]	5.60 ± 0.02	237.6 ± 1.5
e	0.15 ± 0.15	0.19 ± 0.09
ω [°]	30 ± 100	-233 ± 21
K [m s ⁻¹]	6.5 ± 1.0	13.4 ± 1.0
T_0 (periastron) [BJD]	$2454\,637.7 \pm 1.6$	$2454\,193 \pm 13$
$M_P \sin i$ [M _{Jup}]	$0.045 \pm 0.007^\ddagger$	$0.33 \pm 0.03^\ddagger$
$M_P \sin i$ [M _⊕]	$14.4 \pm 2.1^\ddagger$	$104 \pm 10^\ddagger$
a [AU]	$0.056 \pm 0.002^\ddagger$	$0.68 \pm 0.02^\ddagger$
V_r [km s ⁻¹]	53.345 ± 0.001	
σ_{O-C} [m s ⁻¹]	4.3	
reduced χ^2	3.2	
N	83	
span [years]	5.0	

‡: using $M_\star = 0.74 \pm 0.07 M_\odot$

get on a longer time baseline are mandatory to establish or not the presence of the hypothetic planet BD−08°2823d.

The lower panel of Fig. 2 shows the bisector spans as a function of the radial velocities residuals after the 2-planet fit. This does not show an anti-correlation between those two signals, as it could be expected in case of spotted stellar surface due to activity (see, e.g., Melo et al. 2007, Boisse et al. 2009). The absence of anti-correlation, whereas activity is supposed to be here the main part of radial velocity residuals, could be due to the fact that the rotation velocity is low, or to activity processes more complex than simple cool stellar spots. It could also be due to the presence of additional companions (as the hypothetic BD−08°2823d), that would induce radial velocity variations uncorrelated with the bisectors.

We note also that we did not find any anti-correlation between the bisector spans and the radial velocities with either one or the other planet removed. Such anti-correlation with just one planet removed would argue that the other signal is due to activity; this is not the case.

4.2. Fit with stellar activity

In the previous section we have shown a Keplerian fit of the two planets without attempting any fit of the stellar activity jitter signal in the radial velocities. Our knowledge of the activity is poor; for example the number, locations and sizes of potential stellar spots are far to be controlled. We attempt here a naive, phenomenological approach, based on the fact that activity shows signals in the periodograms, so stellar jitter has a periodical nature that is linked to the rotation of the star. Unfortunately these signals are only *quasi-periodical*: they do not reproduce themselves periodically in an identical form for a long time, as all these phenomena have limited life times. Fitting the stellar jitter with sinusoids over the 5-year time span do not provide satisfactory fits.

We thus tried such sinusoid fits on a shorter time span. We chose a 101-day interval, between BJD-2400000 = 54547.5 and 54648.5. This interval has a good sampling (27 measurements), including two 9-night sequences with almost one measurement per night (8 and 9 measurements in the two sequences) at high accuracy (uncertainties between 1.0 and 1.7 m s⁻¹). This should improve the coherence of the stellar jitter in term of periodicity, as well as allowing the 5.60-day-period planet to be well sampled. Using sinusoids of periods near 26 days, we fitted on this 101-day interval the activity indicators studied in

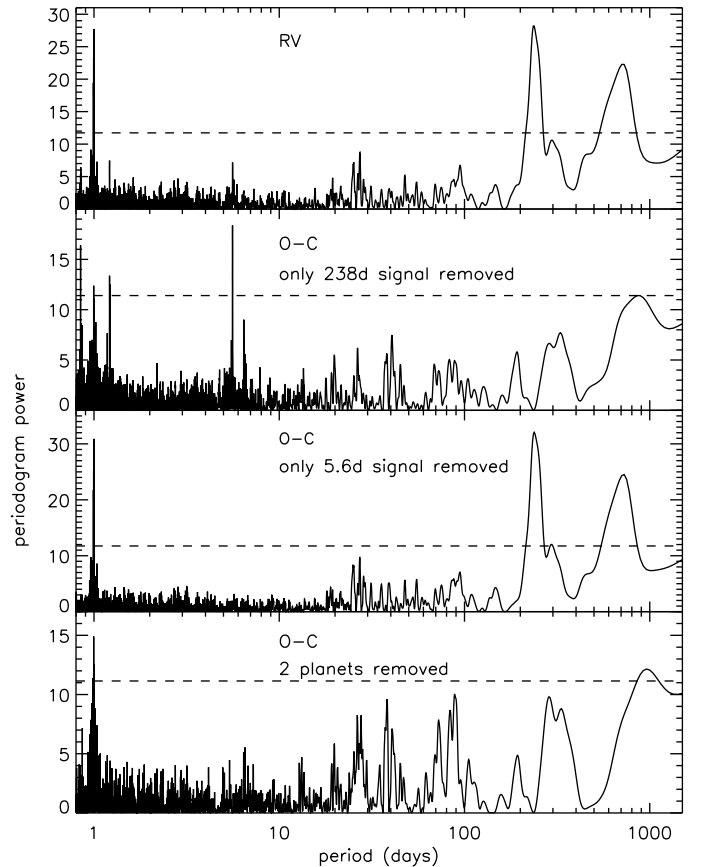


Fig. 5. Lomb-Scargle periodograms of the HARPS radial velocities. The upper panel shows the periodogram computed on the initial radial velocities, without any fit removed. The second and third panels show the periodograms computed on the residuals of the fits including BD−08°2823c or BD−08°2823b only, respectively. The bottom panel shows the periodogram after the subtraction of the 2-planet fit. The horizontal dashed lines correspond to the false-alarm probability of 1×10^{-3} .

Fig. 3, namely the FWHMs, contrasts and bisectors of the CCFs, and the $\log R'_{HK}$ indexes. The best solution we obtained was for a 26.6-day period. Together with the periodograms shown in Fig. 3, this allowed us to determine the rotation period: 26.6 ± 1.5 days. We fitted on the same interval the radial velocities, using Keplerian models for the two planets, and an extra sinusoid to approximate the stellar jitter. The parameters of the inner planet were free, as the mass of the outer one. The period, eccentricity and orientation of the orbit of BD−08°2823c were fixed to the values obtained above, the 101-day interval being too short to constrain this 238-day-period orbit.

The results of these fits agree with those obtained in § 4.1. The fits are plotted in Fig. 6, which shows on the upper panel a good match of the radial velocities and the model, especially on the two high-frequency observation sequences that show the variations due to BD−08°2823b. The lower panels show the activity signals. The 26.6-day-period sinusoids provide acceptable approximations for their variations, which remain however more complex than this simple sinusoid shape. The lower panel shows the stellar jitter only, i.e. the sinusoid that is added to the two

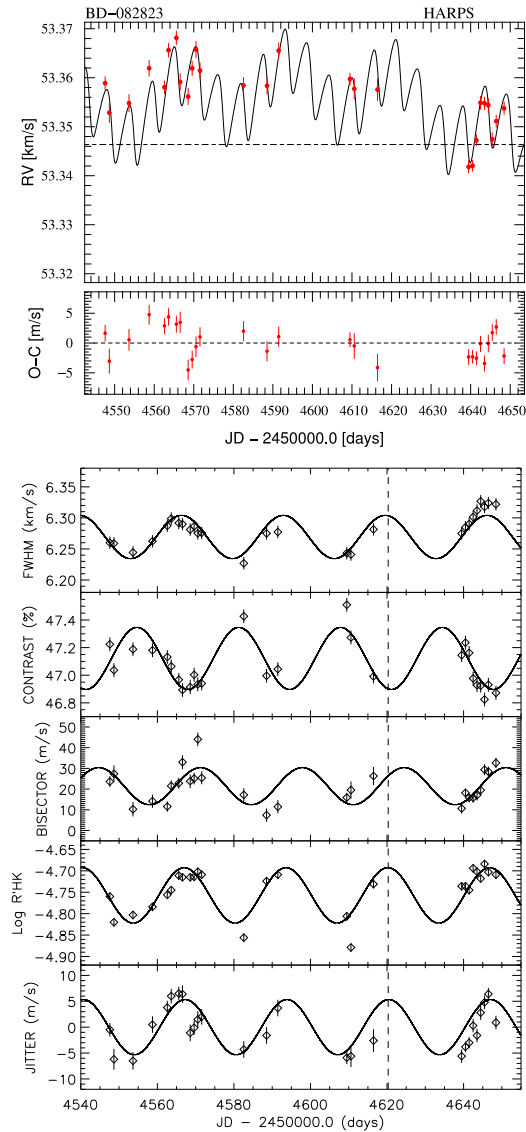


Fig. 6. Fit of the two planets and the stellar activity on a 101-day interval. The *upper plot* shows the HARPS radial velocities of BD−08°2823 with a fit including two Keplerian curves for the planets and a 26.6-day-period sinusoid for the stellar jitter. The *middle plot* shows the residuals of this fits. The *lower plot* shows on five panels the measurements of the FWHMs, contrasts and bisectors of the CCFs, the $\log R'_{\text{HK}}$ and the stellar jitter, respectively from top to bottom. Sinusoid fits with 26.6-day period are overplotted. The stellar jitter in the lower panel is the sinusoid that is added to the two Keplerian in the upper plot. The vertical dashed-line helps visualize the correlations. Error bars at 1σ are plotted for all measurements in this figure.

Keplerian in the upper panel. It has an amplitude of $\pm 5 \text{ m s}^{-1}$. The residuals of the radial velocities fit with two Keplerian and a sinusoid is plotted in the middle panel of Fig. 6. Its dispersion is reduced down to 2.5 m s^{-1} , which is an improvement by comparison to the 4.3 m s^{-1} dispersion obtained on the full dataset in § 4.1 without an attempt to fit the stellar jitter (or 4.1 m s^{-1} dispersion if computed only on the 101-day interval, again without stellar jitter fit). It remains larger than the error bars, because

of the imperfection of the sinusoid model we used for the stellar jitter (and perhaps also because of possible extra planets). We restrained this fit to a single sinusoid for the stellar jitter, without including extra sinusoids at the periods of the stellar rotation harmonics. Indeed, these harmonics are not detected in the radial velocities (see § 3.2 and Fig. 3).

Despite its simplicity, the simple sinusoids allow correlations to be seen between the different parameters on this 101-day time span (Fig. 6, lower panels). The FWHMs and contrasts of the CCFs are anti-correlated, implying spectral line deformations due to activity that let nearly constant their equivalent widths. This could be understood as the surface of the CCF is an indicator of the stellar metallicity (Santos et al. 2002). The velocity jitter is barely correlated with $\log R'_{\text{HK}}$, as well as with the FWHM and the bisector of the CCF. The correlation between the FWHM and $\log R'_{\text{HK}}$ is different from what was seen for example in the case of the spotted star CoRoT-7, for which those two values are rather anti-correlated (Queloz et al. 2009). Also, the apparent correlation between $\log R'_{\text{HK}}$ and the radial velocity jitter is different from the picture seen in the cases of the active stars HD 166435 (Queloz et al. 2001), GJ 674 (Bonfils et al. 2007) or HD 189733 (Boisse et al. 2009). And finally, there is an apparent correlation between the bisector and the radial velocity jitter on this 101-day time span, possibly with a small phase offset (see Fig. 6). This possible correlation is also shown on the lower panel of Fig. 2. All these relations drawn a picture for BD−08°2823 activity that is quite different from a simple scenario where the radial velocity jitter is mainly due to dark spots on the stellar surface that modulate the shape of the lines as the star is rotating. Other phenomena are likely to occur on this star; they may include pulsations, convections, flares, plages, hot spots...

The effect of the stellar activity on the observed radial velocities of BD−08°2823 is of the order of 4 m s^{-1} . This is lower than the semi-amplitudes measured for the two detected planets, but not negligible. The error bars reported in Table 3 were derived from χ^2 variations and Monte Carlo experiments with and without stellar activity modeling, as well as from trials and errors with different kinds of sinusoids for the stellar jitter. Our poor understanding of the stellar activity of BD−08°2823 put us to remain cautious on the obtained error bars. The reality of the two planets in this range of mass is however well established, their signatures being clearly detected at two periods that show no signals linked to stellar activity.

5. Discussion

Finding transiting planets in the *Hipparcos* epoch photometry annex does not look promising. Our attempt for *a-priori* detections did not succeed, and up to now, only two *a-posteriori* detections were performed within the *Hipparcos* data, in the cases of HD 209458b and HD 189733b that were first revealed from ground observations. Three main limitations make it difficult. First, the error bars on individual photometric measurements are of the same order of magnitude than the expected signal for transits of giant planets, or even slightly larger. Second, the sparse time-coverage allows only a few points to be obtained in a potential transit. These two limitations make any transit identification at the limit of detection. Third, stellar activity could produce false positives, which are difficult to identify with the sparse time-coverage. The ESA mission Gaia (Perryman et al. 2001) is awaited as the successor of *Hipparcos*. Its potential for planetary transit discoveries in front of bright stars could be considered, as its sensitivity and accuracy would be better

than *Hipparcos*. However, the time coverage won't be better than that of *Hipparcos*, which will prohibit well-resolved light curve studies. Stellar activity should thus also be a limitation for transit detections with Gaia. Dedicated surveys have proven to be more efficient for transit detections. Ground-based programs allow Jupiter-size planets to be detected, with improving accuracies that now point toward planets with smaller radii (Bakos et al. 2009), whereas space-based programs allow planets with even smaller radii to be detected (Léger et al. 2009, Queloz et al. 2009), as well as planets on longer periods (Moutou et al. 2009b). If accepted, the ESA-proposed space mission PLATO (Catala et al. 2009) could permit the detection of such kind of transiting planets in front of brighter stars.

If this search in the *Hipparcos* data did not provide any detection of new transiting planets, it allowed the serendipitous discovery of a new planetary system around BD−08°2823. This target was first identified as presenting promising radial velocity variations, in which we identified the signature of two new extra-solar planets thanks to an intensive monitoring with HARPS. The inner planet, BD−08°2823b, is a hot-Neptune with a minimum mass of $14.4 M_{\oplus}$. Its 5.60-day orbit could be circular or slightly eccentric. The outer planet, BD−08°2823c, is slightly more massive than Saturn, with a minimum mass of $0.33 M_{\text{Jup}}$. Its orbit is moderately but significantly eccentric, and has a period of 237.6 days. As the masses are low and the orbits are distant and nearly circular, the mutual interactions between the two planets are negligible.

The reflex motions that these two planets induce to their host star have semi-amplitudes of 6.5 and 13.4 m s^{-1} , which can be distinguished from the 4-m s^{-1} jitter due to stellar activity. We summarize here the arguments that allow us to conclude that these two signals are due to planets and not to stellar activity:

- the signals with periods of 5.60 and 237.6 days are seen only in the radial velocities, and are not seen in the shapes of the lines nor in the activity indexes;
- these two periods do not correspond to the rotation period of the star, nor to its harmonics or its aliases;
- with the available data, the signal is coherent over the 5-year time span of the observations.

The radial velocities can be fitted on a short time span by two Keplerian and a sinusoid that models the stellar activity. Acknowledging that we do not have a good understanding of the stellar activity processes, we can alternatively fit the radial velocities using two Keplerian only. By doing that we assume that the stellar jitter is damped and averaged out over the 5-year time-span, and would only lead to a dispersion of the residuals of the fit that are larger than expected from the accuracy of the radial velocity measurements. Additional planetary companions are possible in this system, so the monitoring of BD−08°2823 should be continued.

Most of the Neptune-mass and Super-Earth planets found by the HARPS GTO program are detected from a survey of about 200 non-active solar-type stars. They are monitored with numerous high-precision measurements, using simultaneous thorium calibration and exposures of 15-minute duration to average out the stellar oscillations (Santos et al. 2004b, Udry et al. 2006, Lovis et al. 2006, Bouchy et al. 2009, Mayor et al. 2009). This is not the case for BD−08°2823b, that was discovered from lower signal-to-noise exposures, without simultaneous calibration, and as a serendipitous result of a program that preferentially selected active stars. BD−08°2823 is one of the most active stars around which a low-mass planet have been found, together with CoRoT-7 (Queloz et al. 2009) and a few M-dwarfs

(Bonfils et al. 2007, Forveille et al. 2009). Those cases support the fact that active stars should not be neglected in exoplanet hunts, even when searching for low-mass planets.

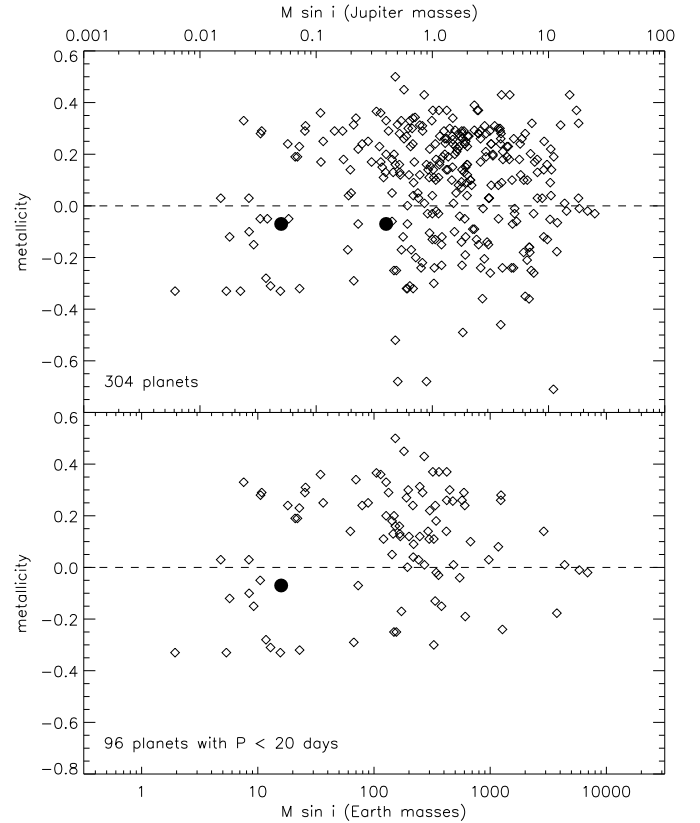


Fig. 7. Stellar metallicities as a function of the planetary masses, for 304 known extra-solar planets (*top*), and for the 96 ones among them with orbital periods shorter than 20 days (*bottom*). BD−08°2823b and BD−08°2823c are indicated by the filled circles. Giant planets are preferentially hosted by stars with higher metallicities than low-mass planets.

BD−08°2823 has a metallicity that is slightly lower than that of the Sun. This strengthens the fact that whereas giant planets are more frequently found around stars with supersolar metallicities, this tendency is not seen for Neptune-mass nor Super-Earth planets. This is shown in Fig. 7, that presents the minimum masses of known exoplanets as a function of the metallicity of their hosting stars. The data are taken from the compilation of the Extrasolar Planets Encyclopedia¹. While planets with masses larger than $1 M_{\text{Jup}}$ are more numerous around overmetallic stars, there are clearly more numerous around undermetallic stars for planetary masses below $20 M_{\oplus}$. The same effect is seen if we select only the planets with orbital periods of 20 days or shorter, i.e. in the period regime where most of the low-mass planets are detected up to now (lower panel of Fig. 7). Indeed, among the ~ 30 planets with a projected mass lower than $0.1 M_{\text{Jup}}$, only four have orbital periods longer than 20 days (namely Gl 581d, HD 40307d, HD 69830c and d).

¹ <http://exoplanet.eu>

Planet formation models based on the core accretion scenario (Mordasini et al. 2009a, 2009b) have shown that the sharply rising probability of detecting giant planets with stellar metallicity can be at least partially accounted for by the fact that metal rich systems favor the formation of massive planets and that the radial velocity technique is most sensitive to massive bodies. Observations also seem to indicate that this correlation vanishes for Neptune-mass planets, a trend also found in population synthesis calculations (Mordasini et al, in preparation). These calculations even show that the correlation reverses for very small planetary masses ($< 3 - 5 M_{\oplus}$), a prediction that will have to be confirmed by observations. In fact, a careful analysis of the theoretical models indicate that the critical parameter is the overall mass of heavy elements rather than the metallicity. Since this mass is determined by the metallicity and the mass of the initial proto-planetary disk (which is unknown), it makes a straight interpretation more difficult. For example, models predict that low mass objects orbiting metal rich stars or relatively massive planets orbiting metal poor stars are also possible albeit they should be rare.

The BD−08°2823 system also agrees with the tendency of low-mass planets to be preferentially found in multiple systems. Almost 70 % of the ~ 30 planets with projected masses lower than $0.1 M_{\text{Jup}}$ are found in multiplanet systems, whereas this ratio is only ~ 25 % for all the ~ 350 known planets. Considering again only the known planets with orbital periods shorter than 20 days, less than ~ 20 % of them are found to be in multiplanet systems: those ~ 20 % are mainly low-mass planets.

No photometric search for transits have been managed for BD−08°2823 from follow-up ground-based observations; depending on the unknown inclination i of the orbit, the transit probability for BD−08°2823b is about 9 %. Its expected depth is out of reach of the *Hipparcos* photometric accuracy.

Acknowledgements. We would like to thank F. Pont, F. Arenou, I. Boisse, X. Bonfils, J.-M. Désert, R. Ferlet, J. Laskar, D. Sosnowska and A. Vidal-Madjar for helps and discussions, as well as the different observers from other HARPS programs who have also measured BD−08°2823. We are grateful to the ESO staff for their support on the HARPS instrument. GH, FB and ALDE acknowledge support from the French National Research Agency (ANR-08-JCJC-0102-01). DE acknowledges financial support from the CNES. NCS would like to thank the support by the European Research Council/European Community under the FP7 through a Starting Grant, as well from Fundação para a Ciência e a Tecnologia (FCT), Portugal, through programme Ciência 2007, and in the form of grants reference PTDC/CTE-AST/098528/2008 and PTDC/CTE-AST/098604/2008.

References

Bakos, G. A., Torres, G., Pál, A., et al. 2009, ApJ, submitted [arXiv:0901.0282]
 Baranne, A., Queloz, D., Mayor, M., et al. 1994, A&AS, 119, 373
 Boisse, I., Moutou, C., Vidal-Madjar, A., et al. 2008, A&A, 495, 959
 Bonfils, X., Mayor, M., Delfosse, X., et al., A&A, 474, 293
 Bouchy, F., Udry, S., Mayor, M., et al. 2005, A&A, 444, L15
 Bouchy, F., Queloz, D., Deleuil, M., et al. 2008, A&A, 482, L25
 Bouchy, F., Mayor, M., Lovis, C., et al. 2009, A&A, 496, 527
 Castellano, T., Jenkins, J., Trilling, D. E., Doyle, L., & Koch, D. 2000, ApJ, 532, L51
 Catala, C., 2009, ExA, 23, 329
 Desort, M., Lagrange, A.-M., Galland, F., Udry, S., Mayor, M. 2007, A&A, 473, 983
 Desort, M., Lagrange, A.-M., Galland, F., Beust, H., Udry, S., Mayor, M., Lo Curto, G. 2008, A&A, 491, 883
 Fernandes, J., Santos, N. C. 2004, A&A, 427, 607
 Forveille, T., Bonfils, X., Delfosse, X., et al. 2009, A&A, 493, 645
 Hébrard, G., & Lecavelier des Etangs, A. 2006, A&A, 445, 341
 Jenkins, J. M., Caldwell, D. A., & Borucki, W. J. 2002, ApJ, 564, 495
 Lagrange, A.-M., Desort, M., Galland, F., Udry, S., Mayor, M. 2009 A&A, 495, 335
 Laughlin, G. 2000, ApJ, 545, 1064

Léger, A., Rouan, D., Schneider, J., et al., 2009, A&A, 506, 287
 Lovis, C., Mayor, M., Pepe, F., et al. 2006, Nature, 441, 305
 Mamajek, E. E., & Hillenbrand, L. A. 2008, ApJ, 687, 1264
 Mayor, M., Pepe, F., Queloz, D., et al. 2003, Msngr., 114, 20
 Mayor, M., Udry, S., Lovis, C., et al. 2009, A&A, 493, 639
 Melo, C., Santos, N. C., Gieren, W., et al. 2007, A&A, 467, 721
 Mordasini, C., Alibert, Y., Benz, W. 2009a, A&A, 501, 1139
 Mordasini, C., Alibert, Y., Benz, W., Naef, D. 2009b, A&A, 501, 1161
 Moutou, C., Mayor, M., Lo Curto, G., et al. 2009a, A&A, 496, 513
 Moutou, C., Bruntt, H., Guillot, T., et al. 2009b, A&A, 488, L47
 Noyes, R. W., Hartmann, L. W., Baliunas, S. L., Duncan, D. K., Vaughan, A. H. 1984, ApJ, 279, 763
 Pepe, F., Mayor, M., Galland, F., et al. 2002, A&A, 388, 632
 Pepe, F., Mayor, M., Queloz, D., et al. 2004, A&A, 423, 385
 Perryman, M. A. C., Lindegren, L., Kovalevsky, J., et al. 1997, A&A, 323, L49
 Perryman, M. A. C., de Boer, K. S., Gilmore, G., et al. 2001, A&A, 369, 339
 Pont, F., Bouchy, F., Melo, C., Santos, N. C., Mayor, M., Queloz, D., & Udry, S. 2005, A&A, 438, 1123
 Press, W. H., Teukolsky, S. A., Vetterling, W. T., & Flannery, B. P. 1992, Numerical recipes in C. The art of scientific computing, 2nd (Cambridge: University Press)
 Queloz, D., Henry, G. W., Sivan, J. P., et al. 2001, A&A, 379, 279
 Queloz, D., Bouchy, F., Moutou, C., et al. 2009, A&A, 506, 303
 Robichon, N., & Arenou, F. 2000, A&A, 355, 295
 Santos, N. C., Mayor, M., Naef, D., et al. 2000, A&A, 361, 265
 Santos, N. C., Mayor, M., Naef, D., et al. 2002, A&A, 392, 215
 Santos, N. C., Israelian, G., Mayor, M. 2004a, A&A, 415, 1153
 Santos, N. C., Bouchy, F., Mayor, M., et al. 2004b, A&A, 426, L19
 Söderhjelm, S. 1999, Informational Bulletin on Variable Stars, 4816, 1
 Udry, S., Mayor, M., Benz, W., et al. 2006, A&A, 447, 361

Appendix A: Selection of targets for transiting planets search in the *Hipparcos* database

We present in this Appendix the systematic search we managed in the *Hipparcos* epoch photometry for planetary transit candidates (§ 2).

First, we selected 23 304 stars among the 118 204 of the *Hipparcos* epoch photometry catalog, according to the following criteria:

- $B - V > 0.4$ (F2 type and later);
- $\pi > \sigma_{\pi}$ (defined parallax);
- empty H48 field (reference flag for photometry);
- H52 field different from D, P, or R (variability types);
- $R_{\star} < 2 R_{\odot}$ (small stellar radius).

Then we kept only targets with at most one epoch brighter than 3σ from the average magnitude (in order to remove remaining variables) and at least 40 different available epochs. We performed the periods' research on the 17 800 remaining stars.

For each target, we took the two faintest epochs and we scan all the possible periods in order to have those two points in a transit. Then we adopted the period producing the lowest flux in the drop, and we quantified this solution with the parameter α , defined as:

$$\alpha = \frac{\langle V_{\text{in}} \rangle - \langle V_{\text{out}} \rangle}{\sqrt{\sigma_{\langle V_{\text{in}} \rangle}^2 + \sigma_{\langle V_{\text{out}} \rangle}^2}}$$

where $\langle V_{\text{in}} \rangle$ and $\langle V_{\text{out}} \rangle$ are the averaged magnitudes of the epochs respectively in and out the drop, and σ the standard deviations. The higher α is, the deeper and more significant the drop is. We also computed the χ^2 for the fit of the epochs in the drop with a transit curve for a planet with a radius $R_p = (0.11 \pm 0.04) R_{\odot}$, implying a $\Delta V_{0.11}$ drop in magnitude:

$$\chi^2 = \sum_{\text{transit}} \frac{(V_i - \langle V_{\text{out}} \rangle - \Delta V_{0.11})^2}{\sigma_{V_i}^2 + \sigma_{\langle V_{\text{out}} \rangle}^2 + \sigma_{\Delta V_{0.11}}^2}$$

We finally computed the goodness of fit (gof) for this χ^2 . The selection of candidates is based on those two parameters: α and the goodness of fit.

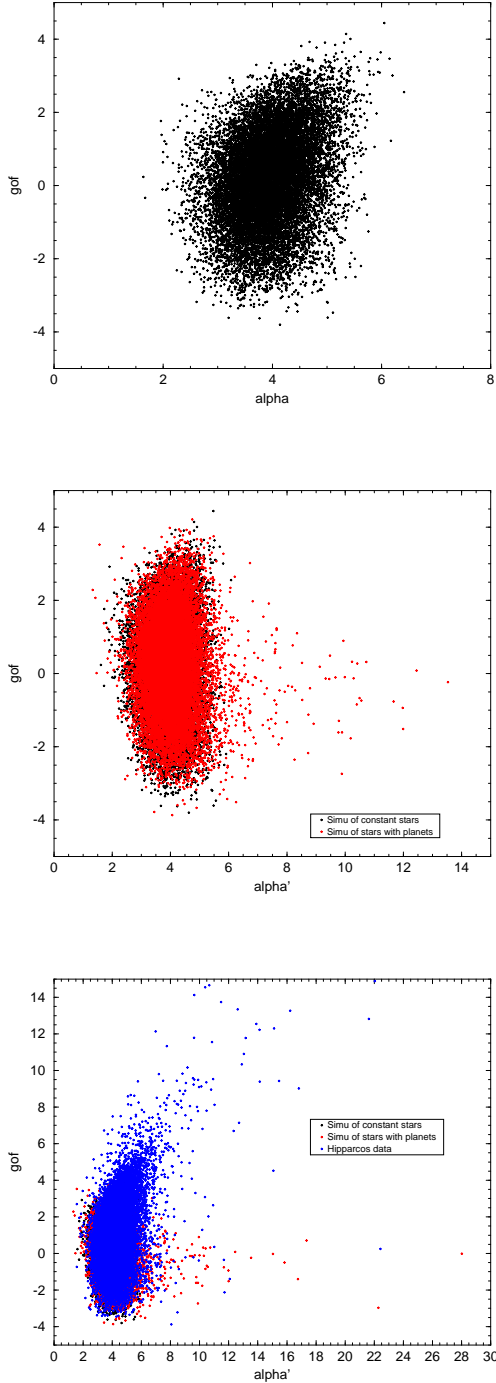


Fig. A.1. Threshold tuning simulations. The parameters α and α' characterize the depth and the significance of the transit, and gof the goodness of fit. These parameters are defined in the text. *Top:* Constant stars. *Middle:* Constant stars (black) and stars with transits (red). *Bottom:* Actual data (blue) and simulations for constant stars (black) and stars with transits (red).

We performed two simulations in order to tune the threshold: for the 17 800 stars selected above, we assumed in the first simulation that all the stars are constant, whereas in the second simulation, we assumed that all the stars host a transiting planet with a radius chosen randomly within $0.07 - 0.15 R_{\odot}$. We kept the individual error on the photometry on each epoch.

The upper panel of Fig. A.1 shows the goodness of fit as a function of α for the first simulation. The distribution is skew as α and the goodness of fit are correlated. In order to make easier the selection, we fitted the distribution with a line, and computed α' , which is corrected (with a first-order polynomial) from this skew. The middle panel of Fig. A.1 shows the goodness of fit as a function of α' for the two simulations. $\alpha' > 5.3$ appears to be an appropriate threshold for transit candidates selection: indeed, 127 and 489 stars are above this limit in the first and second simulation, respectively. We can thus estimate to $(489 - 127)/17800 = 2\%$ the detection rate. With 0.06% chance that a given star harbors a transiting extra-solar planet, the 17800 targets of our latest sample should include ~ 11 transiting planets. The expected transiting planet detection number with our method should thus be slightly less than unity ($11 \times 2\% = 0.2$).

The actual data for the 17800 selected targets are plotted in the lower panel of Fig. A.1. The stars with high α' and high goodness of fit are eclipsing binaries that were not identified in the *Hipparcos* catalog. In order to remove those binaries, we removed targets with goodness of fit larger than 2.5. We also removed targets with $R_* > 1.3 R_{\odot}$, and obtained a list of candidates, sorted by decreasing α' .

Targets referenced in SIMBAD as binaries, active, or variable stars were removed from the obtained list, as well as targets with already known planets at the time of the observing run (HD 70642, HD 39091, HD 10647, HD 4208, HD 17051, HD 13445, HD 75289, and HD 83443 – we checked that the *Hipparcos* photometric data did not include periodic variations at their periods).

Using HARPS, we performed follow-up observations of 194 of these selected targets in December 2004, as part of the program 074.C-0364. The apparent magnitudes of the observed stars range from 4.9 to 11.5. Exposures of typically a few minutes duration were obtained, allowing 70 to 90 targets to be observed each night. Errors on the measured radial velocities are typically of the order of 2 m/s. In order to identify hot Jupiters, targets were removed from the candidate list after one, two, or three observations, according to the following observational strategy:

- observations were stopped after one HARPS measurement if: 1) there are two peaks in the CCF; only one SB2 was found during our observations (HD 23919), binaries having been previously removed from the candidate list from *Hipparcos* flags and SIMBAD checks; 2) the full width at half maximum of the CCF is larger than 15 km/s, which prohibit accurate radial velocity measurements (17 stars);
- observations were stopped after two HARPS measurements if: 1) the radial velocity difference ΔRV between the two measurements is larger than 2.5 km/s (no SB1 were found); 2) $\Delta RV < 5$ m/s (113 stars);
- observations were stopped after three HARPS measurements if $\Delta RV < 20$ m/s (26 stars).

Radial velocity variations larger than 20 m s^{-1} were measured for 37 stars, i.e. 19% of our observed sample. However, those variations are mainly caused by stellar activity (see § 2).